DESIGN AND FABRICATION OF THE COMPACT-ERL MAGNETS*

A. Ueda†, K. Harada, S. Nagahashi, T. Kume, M. Shimada, T. Miyajima, N. Nakamura, K. Endo,
High Energy Accelerator Research Organization (KEK), Tsukuba, Ibaraki 305-0801, Japan

Abstract

The compact Energy Recovery Linac (cERL) was constructed and operated at KEK. For the cERL we designed and fabricated the eight main bending magnets, fifty seven quadrupole magnets, four sextupole magnets and sixteen small bending magnets [1]. These magnets are used at 3 MeV (for low energy part) and 20 MeV (high energy part) beam energy now, but we designed them to be used for maximum 10 MeV and 125 MeV beam energy for future upgrade of the cERL. The magnetic field analysis was done by 2D and 3D simulation code (OPERA) to design magnet shape. The main bending magnets and quadrupole magnets are made of electromagnetic steel sheet and the other magnets are made of electromagnetic soft iron. In this paper, we show the detail of the designing and fabricating work of those magnets.

INTRODUCTION

The cERL was constructed in 2013 and started operation in 2014. Now we have been commissioned continuously [2].

At the cERL, electron beam that generated by the photocathode electron gun are accelerated by the injector linac and the main linac. They go around two arc sections, and return to the main linac. Then they are decelerated, and ejected to beam dump. The Illustration of the cERL is shown in Fig 1.

In November 2015, four sextupole magnets were installed in the two arc sections for the demonstration of bunch compression. And during beam commissioning in March 2016, we operated bunch compression mode and measured bunch lengths by OTR in the south straight section just after the first arc [3].

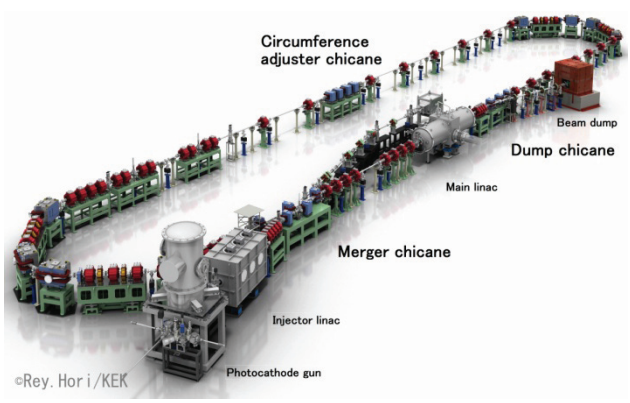

Figure 1: Illustration of the Compact ERL.

* Work supported by "A government (MEXT) subsidy for strengthening nuclear "of Japan
† akira.ueda@kek.jp

BENDING MAGNETS

There are eight main bending magnets and sixteen small bending magnets in the cERL. Parameters of the bending magnets are shown in Table 1.

Main Bending Magnets

Main bending magnets are trapezoidal shaped sector type magnets. Their bending radii are 1m, and bending angles are 45degree. The magnetic core consists of the lamination of the silicon steel. The edge was cut in order to form sector shape after bonding laminated steel.

Shape of the magnet cross section was decided by 2D simulation to obtain the required good field region (G.F.R.). These magnets have a large sagitta and the required G.F.R. [$\Delta By/By_0 \leq \pm 5E\text{-}4$] is about 150 mm.

To obtain the required G.F.R., the shims [4] that are trapezoidal extensions above the pole faces, were optimized by 2D simulation [5].

We need to use these magnets from low energy to high energy. But magnetic permeability of the steel is lower at low field region, and using low permeability steel, G.F.R. reduces. Therefore, we selected NSSMC 50H250 steel [6] that is relatively high permeability at low field.

The edge effects of the magnet were compensated by end shims made of rectangle steel attached both ends of the magnet faces. The shape of the end shim is designed by 3D simulation to obtain the integral G.F.R. over 150 mm.

The main bending magnets photo and Opera model are shown in Fig 2.

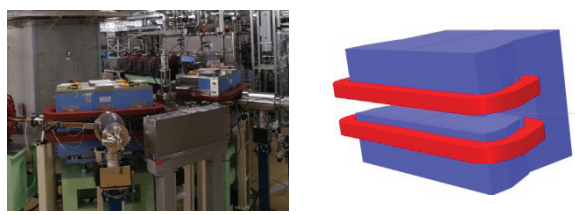

Figure 2: main bending magnets at second arc section (left) and opera model (right).

Small Bending Magnets

Sixteen small bending magnets are used for injecting an electron beam from an injector, ejecting a decelerated beam to its dump and adjusting the circumference of the recirculation loop.

The magnetic core of these magnets consists of the electromagnetic soft iron (NSSMC NS-MIP250N) instead of the silicon steel because each type of the magnets has a different cross section shape.

In general, the magnetic property of the electromagnetic soft iron is deteriorated by mechanical processing, and at the low field region, that deterioration becomes significant large.

ISBN 978-3-95450-147-2

Table 1: Parameters of the Bending Magnets

Magnet type	Number of magnets	Core WxHxL [mm]	Gap Height [mm]	Pole Width [mm]	Maximum current [A]	Coil turn numbers	Maximum magnetic field [T]	Good field region [mm]
Main Bend	8	490x540x820	60	230	100	28x2	0.817	150
Merger A	3	420x320x200	70	180	10	95x2	0.0456	80
Merger B	1	410x335x200	60	215	10	82x2	0.0498	30
Merger C	1	420x385x200	70	180	10	190x2	0.0925	115
Dump A	2	425x325x300	70	195	10	79x2	0.0351	95
Dump B	1	435x345x300	70	195	10	158x2	0.0701	95
Circumference adjuster chicane	4	440x450x300	70	240	30	184x2	0.248	140

And it is necessary to do magnetic annealing that keeps 890 degrees for 1 hour, if we want to recover the characteristic of magnetic permeability [7].

In the cERL the chicane magnets are excited to about 0.1 T, the magnetic permeability of these magnets is degraded about 50%. So we decided to perform magnetic annealing at the last process of the magnet fabrication.

However, it was necessary to consider the possibility that the gap height became larger than its tolerance [±50μm] by transformation due to the magnetic annealing. We measured transformation before and after the magnetic annealing by using test block. We concluded that the transformation is so small that the gap height is within its tolerance after magnetic annealing.

We also designed the shape of the magnet using 2D and 3D magnetic simulation, and the magnet pole with shims were optimized and end shims were attached on the both ends of the magnets to obtain required integral G.F.R.

Measured magnetic field for Magnet No.2 of Merger A was shown in Fig. 3. The integral magnetic field distribution from the 3D simulation corresponds reasonably well with measurements by a flip-flop coil method [8].

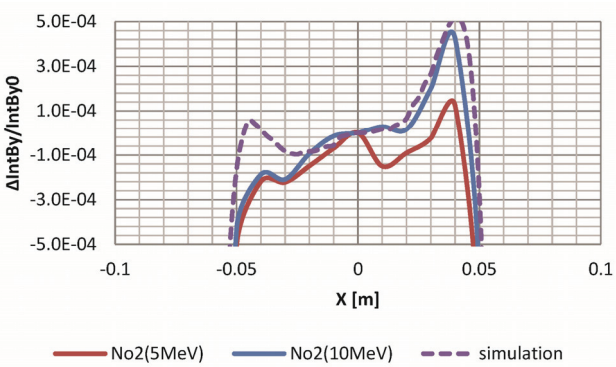

Figure 3: magnetic field measurement for Magnet No.2 of Merger A. Simulation corresponds reasonably well with measurement.

Trajectory and Fringe Field Integral

At the ERL, the electron beam are accelerated by the main linac, and decelerated by the same main linac for the energy recovery. We need to adjust the circumference for efficient energy recovery. To estimate orbit length in the bending magnets, trajectories are calculated using Opera 3D code. By using those results, coordinates of the magnets were decided to adjust the circumference precisely.

Fringe field integrals [9] were calculated from the field map of the 3D magnets simulation. Those results were utilized as a basic parameter of the orbital calculation code.

QUADRUPOLE MAGNETS

We made two types of quadrupole magnets, 100mmQ for the low energy part and 200mmQ for the high energy part. The magnetic core consists of the lamination of the silicon steel (NSSMC 50H250) [6]. The core shapes of both magnets were the same, so they made by using same press die. Parameters of the quadrupole magnets are shown in Table 2.

We designed the quadrupole magnets shape in the same way as the bending magnets. The shape of the magnet cross section was optimized by 2D simulation. Tangential shims [4] on the pole surface were optimized to obtain required G.F.R. and to compensate the edge effects, the end shims were attached to both ends of the magnets. The 100 mm type quadrupole magnets were shown in Fig. 4 (left) and its opera model was shown in Fig. 4 (right).

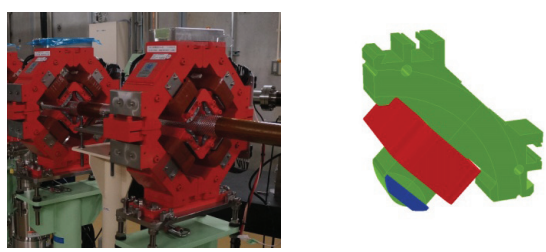

Figure 4: 100mmQ after merger section (left) and opera model (right). The end shim is described in blue.

Table 2: Parameters of the Quadrupole and Sextupole magnets

Magnet type	Number of magnets	Core length [m]	Bore diameter [mm]	Maximum current [A]	Coil turn numbers	Maximum magnetic field gradient	Good field region [mm]
100mmQ	13	0.1	60	5	240/pole	4.545[T/m]	50
200mmQ	44	0.2	60	100 (high energy)	25/pole	8.310 [T/m]	50
				5 (low energy)	280/pole	4.622[T/m]	
SX	4	0.1	70	10	100/pole	166.78 [T/m^2]	60

For optimising the tangential and end shim, we estimate directly width of the G.F.R. [$\Delta B'y/B'y_0 \leq \pm 5E\text{-}4$] from the field map of the magnetic simulation not to estimate harmonics of the field. The estimated G.F.R. is shown in Fig 5. The left side of the figure is 2 dimensional G.F.R. with and without the tangential shim of which start point is 25.2 mm. Similarly the right side is 3 dimensional integral G.F.R. for 200mmQ with and without the end shim having the cutting width of 18 mm and thickness of 5 mm. They show that the tangential and end shims are effective to extend G.F.R.

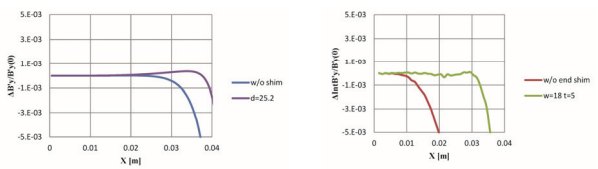

Figure 5: G.F.R. with and without tangential shim (left) and integral G.F.R. for 200mmQ with and without end shim (right). G.F.R is extended by each shim.

SEXTUPOLE MAGNETS

We installed the sextupole magnets in November 2015 to use for the bunch compression. The magnetic core of these magnets consists of the electromagnetic soft iron (NSSMC NS-MIP250N). For the fabrication, we perform magnetic annealing after mechanical processing to recover the characteristic of magnetic permeability in the same way as the small bending magnets of the cERL. The parameters of the sextupole magnets are shown in Table 3.

We designed the shape of the magnet cross section in the same way as the quadrupole magnets to estimate directly width of the G.F.R. [$\Delta B''y/B''y_0 \leq \pm 5E\text{-}3$] by the field map of the 2D simulation, and optimized the tangential shims shape. But for deciding of the end shim, we optimized their shape to minimize their allowed harmonics. Because of deriving second derivatives of the field, the error becomes extremely large, so we couldn't estimate integral G.F.R. properly.

The shape of the end shim for the sextupole magnet is similar to the quadrupole magnets (see Fig. 4 right). We calculated the harmonic of the magnetic field as a function of the thickness (d) and the width of the bottom (w) of the end shim.

Allowed harmonics a6 and a10 divided by fundamental a3 are shown in Fig.6. We calculated 3 cases, w=36.5 mm, 38 mm, and 40 mm. Each cases has a thickness that a6/a3 became nearly zero (see. Fig5 (left)), d=3.5 mm for w=36.5, d=4 mm for w=38 mm and 40 mm. Then a15/a3 became smaller at w=36.5 mm and d=3.5 mm than the other cases (see Fig 5(right)). So we decided the end shim for the sextupole magnet was w=36.5 mm and d=3.5 mm.

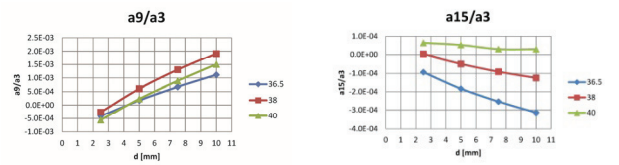

Figure 6: allowed harmonics a9/a3 (left) and a15/a2 (right) for several end shim shape. Case of w=36.5 mm and d=3.5 mm is the smallest.

CONCLUSION

We designed and fabricated the eight main bending magnets, fifty seven quadrupole magnets, four sextupole magnets and sixteen small bending magnets for the cERL.

The shapes of the magnet cross sections were designed to obtain required G.F.R. by 2D simulations and the end shims to compensate the edge effect were optimized by 3D simulations.

Trajectory in the magnets and the fringe field integrals were calculated for deciding coordinates of the magnets, and to use for a basic parameter of the orbital calculation code.

The small bending magnets and sextupole magnets consist of the electromagnetic soft iron, which is significantly deteriorated by mechanical processing at the low field region. To recover the deterioration, magnetic annealing was adopted after mechanical processing.

REFERENCES

[1] K. Harada et al., "The Magnet and Power Supply System for the Compact –ERL", Proc. of IPAC'15, Richimond, VA, USA, p. 2899 (2015).

[2] T.Obina et al., "Recent Developments and Operational Status of the Compact ERL at KEK", in these proceedings, TUPOW036.

[3] M.Shimada et al.,"Bunch compression at the recirculation loop of Compact ERL", in these proceedings, TUPOW038.

[4] N. Marks, "CONVENTIONAL MAGNETS -I", CAS, Zakopane, Oct 2006.

ISBN 978-3-95450-147-2

[5] A. Ueda et al., "Bending Magnets Design of cERL", Proc. of the 7th Annual Meeting of Particle Accelerator Society of Japan, Himeji, Japan, p. 953 (2010) [in Japanese]

[6] Nippon Steel & Sumitomo Metal Corporation http://www.nssmc.com/product/catalog_download/pdf/D005je.pdf

[7] M.Nishio, NIPPON STEEL & SUMITOMO METAL CORPORATION, private communications.

[8] A. Ueda et al., "Design and Fabrication of the Compact-ERL Chicane Magnets", Proc. of the 12th Annual Meeting of Particle Accelerator Society of Japan, Tsuruga, Japan, p. 674 (2015) [in Japanese]

[9] K. L. Brown, "A First- and Second-Order Matrix Theory for the Design of Beam Transport Systems and Charged Particle Spectrometers" SLAC Report-75, 1982, pp. 116-117.